1 **Establishment of an African green monkey model for COVID-19**

2 Courtney Woolsey[1,2], Viktoriya Borisevich[1,2], Abhishek N. Prasad[1,2], Krystle N. Agans[1,2], Daniel J. Deer[1,2],

3 Natalie S. Dobias[1,2], John C. Heymann[3], Stephanie L. Foster[1,2], Corri B. Levine [1,2], Liana Medina [1,2], Kevin

4 Melody[1,2], Joan B. Geisbert[1,2], Karla A. Fenton[1,2], Thomas W. Geisbert[1,2*], Robert W. Cross[1,2]

5

6 [1]Department of Microbiology and Immunology, University of Texas Medical Branch, Galveston, TX 77555,

7 USA.

8 [2]Galveston National Laboratory, University of Texas Medical Branch, Galveston, TX 77555, USA.

9 [3]Department of Radiology, University of Texas Medical Branch, Galveston, TX 77555, USA.

10

11 *Corresponding author: twgeisbe@utmb.edu

12 **Abstract**

13 Severe acute respiratory syndrome coronavirus 2 (SARS-CoV-2) is responsible for an unprecedented global

14 pandemic of COVID-19. Animal models are urgently needed to study the pathogenesis of COVID-19 and to

15 screen candidate vaccines and treatments. Nonhuman primates (NHP) are considered the gold standard model

16 for many infectious pathogens as they usually best reflect the human condition. Here, we show that African green

17 monkeys support a high level of SARS-CoV-2 replication and develop pronounced respiratory disease that may

18 be more substantial than reported for other NHP species including cynomolgus and rhesus macaques. In

19 addition, SARS-CoV-2 was detected in mucosal samples of all animals including feces of several animals as late

20 as 15 days after virus exposure. Importantly, we show that virus replication and respiratory disease can be

21 produced in African green monkeys using a much lower and more natural dose of SARS-CoV-2 than has been

22 employed in other NHP studies.

Introduction

Severe acute respiratory syndrome coronavirus 2 (SARS-CoV-2), the etiological agent of coronavirus disease 2019 (COVID-19), emerged in Wuhan, China in late 2019 and rapidly swept the globe. As of May 16, 2020, over 4.4 million confirmed cases and 302,000 deaths have been reported worldwide [1]. The COVID-19 crisis has inflicted an immense toll on human health causing profound socioeconomic effects that will linger for years to come.

Vaccines and treatments against SARS-CoV-2 could drastically reduce COVID-19 transmission, saving lives and brightening prospects for economic recovery. No licensed countermeasures currently exist, although a number of clinical trials are underway. While clinical testing is a good predictor of preventative and drug efficacy, caution is warranted with this approach due to the potential for disease enhancement. Vaccine candidates against SARS-CoV-1, including inactivated whole-virus, recombinant DNA subunit, virus-like particle, and live virus vector-based vaccines, induced an immunopathology following immunization and experimental infection of mice, ferrets, and nonhuman primates (NHPs) suggesting hypersensitivity to virus components [2-5]. Given the strong genetic similarity of SARS-CoV-2 and SARS-CoV-1 [6], an appropriate surrogate for human COVID-19 is needed to safely evaluate prophylactics. A careful assessment in animal models could reveal possible immune complications elicited by vaccines and therapies prior to their release to the public. Moreover, animal models could help shed light on important aspects of the disease in ways that are not easily addressed or feasible in humans, such as how the virus spreads and interacts with the host immune system.

An ideal COVID-19 animal model would replicate all facets of human disease. Several animal species including mice, hamsters, ferrets, and NHPs were found to support SARS-CoV-2 replication and displayed varying degrees of non-lethal illness when the virus was delivered into the respiratory tract of these animals [7-13]. While each of these models has utility in the study of COVID-19, NHPs have the closest physiological resemblance to humans allowing a better comparison of host responses to infection. This genetic similarity has also contributed to the increased availability of reagents to perform in-depth analyses of the immune response. Recently, the first studies evaluating the pathogenic potential of SARS-CoV-2 in cynomolgus and rhesus macaques were performed. Rhesus macaques developed pneumonia and clinical signs whereas disease in cynomolgus macaques was fairly mild indicating the former appears to better reflect more severe cases of COVID-19 [10-12]. These results suggest certain NHP species may serve as better models than others for

51 coronavirus infections. For SARS, the disease caused by SARS-CoV-1, African green monkeys (AGMs) were

52 found to support the highest level of viral replication, followed by cynomolgus macaques and rhesus macaques

53 when all three species were challenged in parallel [14]. Only AGMs had notable replication in the lower

54 respiratory tract following SARS-CoV-1 inoculation; necropsy of these animals indicated focal interstitial

55 mononuclear inflammatory infiltrates and edema in the lung consistent with human SARS. As SARS-CoV-1 and

56 SARS-CoV-2 share the same putative host receptor angiotensin-converting enzyme 2 (ACE2) [15, 16], we

57 reasoned that AGMs might serve as a useful model for COVID-19.

58 Here, we infected AGMs with a low passage isolate of SARS-CoV-2 (SARS-CoV-2/INMI1-

59 Isolate/2020/Italy) and evaluated their potential as a model for COVID-19. SARS-CoV-2/INMI1-Isolate/2020/Italy

60 was isolated from the first clinical case in Italy [17] and is the first V clade virus (GISAID) to be experimentally

61 inoculated into NHPs. We demonstrate AGMs mimic several aspects of human disease including a high degree

62 of viral replication and severe pulmonary lesions. This model can be used to conduct pathogenesis studies and

63 to screen potential vaccines and therapeutics.

64

65 **Results**

66 We challenged six adult AGMs with 5.0×10^5 PFU of the Italy isolate of SARS-CoV-2 (SARS-CoV-2/INMI1-

67 Isolate/2020/Italy) by combined intratracheal (i.t.) and intranasal (i.n.) routes (dose divided equally). A cohort of

68 three animals was euthanized at 5 dpi, while the remaining three animals were held indefinitely. Blood from all

69 animals was sampled on days 0, 2, 3, 4, and 5, and continuing with days 7, 9, 12, 15, and 21 for animals held

70 past 5 dpi. No overt clinical signs of disease were observable in any of the animals, other than decreased appetite

71 compared to baseline (0 days post-infection; dpi) in 5/6 animals, and a brief period of elevated body temperature

72 suggestive of fever in two of three animals at 3 dpi (Supplementary Figure 1). A biphasic increase in partial O^2

73 pressures were noted in two animals over the course of the study, but no overt changes in partial CO^2 pressures

74 in any animals were noted (Figure 1-A,B). Transient shifts in leukocyte populations and mild thrombocytopenia

75 were observed in all animals, most prominently during days 2-7 post-infection (Supplementary Table 1, Figure

76 1-C,D,E,F). Markers for renal and hepatic function mostly remained unchanged (< 2-fold increases in ALT, AST,

77 ALP); however, CRP, a marker of acute systemic inflammation, was elevated two to seven-fold in all animals 2-

78 5 dpi (Table 1, Figure 1-G,H,I,J). Thoracic radiographs were taken on -1, 2, 3, 4, 5 dpi, and were shown to be

4

79   inconclusive (Supplementary Figure 2). Gross examination at necropsy of three AGMs at 5 dpi revealed varying

80   degrees of pulmonary consolidation with hyperemia in all monkeys (Figure 2). Lesions were multifocal to locally

81   extensive within each lobe. The most severe lesions were located in the dorsal aspects of the lower lung lobes

82   in all animals. A board-certified veterinary pathologist approximated lesion severity for each lung lobe

83   (Supplementary Table 2) Small intestines in all monkeys were segmentally flaccid and distended with gas and

84   yellow liquid contents. Mild lymphoid enlargement was noted in one of the three monkeys. There were no other

85   significant gross lesions.

86   Histologically, all three AGMs at 5 dpi developed varying degrees of multifocal pulmonary lesions. In the

87   most severely affected monkey, histologic features of pneumonia include acute inflammation centered on

88   terminal bronchioles and numerous multinucleated giant cells with irregularly distributed nuclei. Continuous with

89   the terminal bronchiolitis was evidence of diffuse alveolar damage (DAD) with hyaline membrane formation, type

90   II pneumocyte hyperplasia, pulmonary edema and pulmonary hemorrhage. Occasionally, small fibrous tissue

91   proliferations were noted within the terminal airways reminiscent of bronchiolitis obliterans organizing pneumonia

92   (BOOP)-like lesions. Interstitial pneumonia was noted in the lesser affected regions of the lung along with

93   congestion and increased numbers of alveolar macrophages. In the less affected monkeys, pulmonary lesions

94   lack acute inflammation within the terminal bronchioles; however, interstitial pneumonia is present and in one

95   monkey, multinucleated giant cells with irregularly distributed nuclei were prominently displayed within

96   bronchioles. Colocalization of SARS antigen with pulmonary lesions were demonstrated with antibodies against

97   SARS N protein. Positive immunohistochemical labeling was noted diffusely within the cytoplasm of alveolar

98   macrophages, respiratory epithelium, type I pneumocytes and type II pneumocytes. One animal had only positive

99   immunolabeling in respiratory epithelium. Genomic SARS-CoV2 RNA was detected by i*n situ* hybridization in

100   pneumocytes and associated with the alveolar macrophages within acute inflammation centered on terminal

101   bronchioles (Figure 3).

102   We quantified viral load from mucosal swabs and bronchoalveolar lavage (BAL) fluid collected on

103   procedure days by RT-qPCR and plaque titration (Figure 4). All animals had detectable quantities of vRNA and

104   infectious virus from nasal secretions beginning at 2 dpi, with viral titers ranging from ~2-4 log PFU/mL (Figure

105   4-A,B). Both viral RNA (vRNA) and infectious virus were detected from oral swabs from only three animals

106   (AGM-2, AGM-5, AGM-6) 3 dpi, and persisted in AGM-5 up to 7 dpi (Figure 4-C,D). Infectious virus was only

107   detectable from the rectal swab of a single animal (AGM-3) 3-5 dpi; however, vRNA was also detected from

108   AGM-4 and AGM-5 (Figure 4-E,F). Both vRNA and infectious virus was present in BAL fluid from all animals

109   beginning at 3 dpi (Figure 4-G,H). Neither vRNA nor infectious virus was detected by RT-qPCR of RNA from

110   whole blood or plaque titration of plasma from any animal, indicating a lack of circulating cell-associated or free

111   virus in the peripheral blood (data not shown).

112   Similar to human cases of COVID-19, systemic concentrations of a number of inflammatory cytokines

113   and chemokines were elevated following AGM infection. Serum levels of pro-inflammatory IL-8, IP-10, IL-12, and

114   monocyte chemoattractant protein (MCP-1) peaked at 2 DPI corresponding to subsequent recruitment of

115   monocytes and neutrophils in the blood (Figure 1-D,E, Figure 5-C,D,E,F). Increased secretion of IL-6, IFN-beta,

116   and IL-10was also evident at this time point (Figure 5-A,G,H). Notably, IL-6 is thought to predict respiratory failure

117   in human COVID-19 cases and may serve as an effective immunological biomarker [18]. As IL-6 is a main

118   regulator of acute phase fibrinogen synthesis, and elevated fibrinogen and other coagulation abnormalities are

119   thought to correlate with disease severity in hospitalized patients [19, 20] , we also measured levels of this

120   clotting factor. Fibrinogen levels surged in 4 of 6 monkeys indicating potential coagulation abnormalities in these

121   animals (Figure 5-B). This increase in circulating fibrinogen aligns with our gross pathology findings of substantial

122   hemorrhage in the lung of monkeys euthanized at 5 DPI. Collectively, these results indicate the host response

123   to SARS-CoV-2 infection in AGMs parallels that of humans.

124   Four animals seroconverted against SARS-CoV-2, including all three animals held past 5 dpi, with the

125   earliest detection of anti-SARS-CoV-2 IgG occurring at 5 dpi in AGM-3, AGM-4, and AGM-6 (Figure 6-A). IgG

126   titers peaked at 15 dpi, with AGM-6 exhibiting low titers at 15 and 21 dpi compared to AGM-4 and AGM-5.

127   Neutralizing titers (50% plaque reduction values) ranged from 1:8-1:32 were evident beginning at day 5 in one

128   animal and all three animals followed to the study endpoint (Figure 6, B,C,D,E).

129

130   **Discussion**

131   The emergence of SARS-CoV-2, and its astonishingly rapid evolution from localized outbreak to pandemic threat

132   has emphasized the importance of coronaviruses with regards to human health globally, particularly of those

133   clustering with lineage B betacoronaviruses. Accordingly, a necessity exists for the development of animal

134   models for SARS-CoV-2 which recapitulate the COVID-19 disease phenotype observed in humans. With regard

6

135 to NHPs, efforts to do so have been made using both rhesus and cynomolgus macaques [11-13, 21], with rhesus

136 macaques more closely exhibiting the symptoms of COVID-19 disease in humans. Given that AGMs have shown

137 utility as disease models for a number of respiratory pathogens (i.e., Nipah [22], SARS-CoV-1 [14]), we

138 investigated their suitability as a model for SARS-CoV-2 infection.

139 AGMs challenged with an isolate of SARS-CoV-2 from Italy did not develop overt, debilitating clinical

140 illness; however, changes in leukocyte subpopulations, thrombocytes, and serum markers of acute inflammatory

141 processes indicated a systemic response to infection. Using surgically implanted temperature data loggers we

142 were able to detect elevated body temperatures in two animals 3 dpi, indicative of fever. Moreover, all animals

143 held past 5 dpi seroconverted, with two animals achieving high IgG titers (1:6400). The third animal held to 21

144 dpi never had an anti-SARS-CoV-2 IgG titer above 1:200, suggesting a dampened humoral response in this

145 animal, and that immune arms other than humoral immunity may be important during SARS-CoV-2 infection.

146 Additionally, the potential for re-infection in humans with SARS-CoV-2 has been speculated, but the risk factors

147 or actual incidence are unknown. However, antibody titers to endemic human coronaviruses (e.g., HCoV-229E)

148 are reported to gradually wane and re-infection with the homologous virus has been reported [23, 24].

149 An important aspect of the AGM model for SARS-CoV-2 infection is the development of pronounced viral

150 pneumonia. All AGMs in our study exhibited pulmonary consolidation with hemorrhage, varying in severity

151 between animals and lung lobes. We performed thoracic radiographs on all six SARS-CoV-2-infected AGMs;

152 however, the radiographs while consistent with work on SARS-CoV-2-infected macaques recently published by

153 others [11, 12, 21] did not reflect the degree of lesions and hemorrhage of the lungs seen at necropsy. It is our

154 opinion that the radiographs from our study as well as those from the other COVID-19 NHP studies do not

155 convincingly demonstrate SARS-CoV-2-induced disease. Specifically, opacities and changes observed in

156 radiographs could be nonspecific and due to atelectasis, poor inspiratory effort, and BALS collection procedures.

157 Important to this discussion, the current recommendation in humans is to not even use radiography for the

158 primary diagnosis of COVID-19. Notably, a recent study of 636 ambulatory patients with COVID-19 did not

159 detect any abnormalities in chest X rays of almost 60% of the cases [25]. The use of computed tomography (CT)

160 scanning or even plesmography techniques may be more informative for detailed pulmonary investigations using

161 animal models.

7

162   There was evidence of gastrointestinal involvement in the SARS-CoV-2-infected AGMs, which has been

163   reported in human cases [23], as the putative SAR-CoV-2 entry receptor ACE-2 is expressed in the epithelium

164   of the ileum and colon [26]. However, while all animals in our study exhibited abnormalities within the small

165   intestine, we did not observe signs of gastrointestinal distress during the study course, with the possible

166   exception of decreased appetite in most animals.

167   Our data show that infection of AGMs with SARS-CoV-2 results in the release of inflammatory mediators

168   with similar immune signatures as human cases. Several groups reported that levels of IL-6, IL-8, and IL-10

169   correlate with disease severity in human patients [27, 28]. In this study, we observed increased serum levels of

170   these interleukins as well as other pro-inflammatory cytokines and chemokines elevated in human cases.

171   Moreover, we detected a rise in fibrinogen in a majority of monkeys, another prominent finding in human COVID-

172   10 cases. Fibrinogen is implicated in thrombosis and vascular injury suggesting this discovery warrants further

173   investigation. Together, these results indicate the AGM model can be used to study the host response to COVID-

174   19. The heterologous response of AGMs along with the ability to collect tissues and longitudinal samples permits

175   a detailed study of pathogenesis and immunity to COVID-19.

176

177   **Methods**

178   *Virus*

179   The virus (SARS-CoV-2/INMI1-Isolate/2020/Italy) employed was isolated on January 30, 2020 from the sputum

180   of the first clinical case in Italy, a tourist visiting from the Hubei province of China that developed respiratory

181   illness while traveling [17]. The virus was initially passaged twice (P2) on Vero E6 cells; the supernatant and cell

182   lysate were collected and clarified following a freeze/thaw cycle. This isolate is certified Mycoplasma and FMDV

183   free. The complete sequence was submitted to GenBank (MT066156) and is available on the GISAID website

184   (BetaCoV/Italy/INMI1-isl/2020: EPI_ISL_410545) upon registration. For *in vivo* challenge, the P2 virus was

185   propagated on Vero E6 cells and the supernatant was collected and clarified by centrifugation making the virus

186   used in this study a P3 stock.

187

188 *Animal challenge*

189 Animals were anesthetized with ketamine and inoculated with ~5 × 10^5 PFU of SARS-CoV-2 (SARS-CoV-

190 2/INMI1-Isolate/2020/Italy) with the dose being equally divided between the intratracheal (i.t.) (5.0 ml) and the

191 intranasal (i.n.) (1.0 ml total at 0.5 ml per nostril) routes for each animal. Animals were longitudinally monitored

192 for clinical signs of illness including temperature (measured by surgically implanted DST micro-T small

193 implantable thermo loggers (Star-Oddi, Gardabaer, Iceland), respiration quality, and clinical pathology. All

194 measurements requiring physical manipulation of the animals were performed under sedation by ketamine. All

195 animal studies were approved by the University of Texas Medical Branch (UTMB) Institutional Animal Care and

196 Use Committee and adhere to the NIH Guide for the Care and Use of Laboratory Animals.

197

198 *Radiographic technique*

199 All monkeys were imaged with a portable GE AMX-4+ computed radiography system using a DRTECH detector

200 set at a 36 inch focal film distance. Images were captured and evaluated using the Maven Patient Image Software

201 in ventral dorsal (VD) and right lateral (R LAT) positions at 50 kVp and 12.5mA as previously described [22].

202 Chest radiographs were captured and interpreted by a double board-certified clinical veterinarian and veterinary

203 pathologist and reviewed by a MD board-certified radiologist.

204

205 *RNA isolation from SARS-CoV-2-infected AGMs*

206 On specified procedure days (days 0, 2, 3, 4, 5, 7, 12, 15, 21), 100 μl of blood was added to 600 μl of AVL viral

207 lysis buffer (Qiagen) for virus inactivation and RNA extraction. Following removal from the high containment

208 laboratory, RNA was isolated from blood and swabs using the QIAamp viral RNA kit (Qiagen).

209

210 *Detection of SARS-CoV-2 load*

211 RNA was isolated from blood and mucosal swabs and assessed using the CDC SARS-CoV-2 N2 assay

212 primers/probe for reverse transcriptase quantitative PCR (RT-qPCR)[29]. SARS-CoV-2 RNA was detected using

213 One-step probe RT-qPCR kits (Qiagen) run on the CFX96 detection system (Bio-Rad), with the following cycle

214 conditions: 50°C for 10 minutes, 95°C for 10 seconds, and 45 cycles of 95°C for 10 seconds and 55°C for

215 30 seconds. Threshold cycle (C_T) values representing SARS-CoV-2 genomes were analyzed with CFX Manager

9

216 Software, and data are presented as GEq. To generate the GEq standard curve, RNA from Vero E6 cells infected

217 with SARS-CoV-2/INMI1-Isolate/2020/Italy was extracted and the number of genomes was calculated using

218 Avogadro's number and the molecular weight of the SARS-CoV-2 genome.

219   Virus titration was performed by plaque assay with Vero E6 cells (ATCC CRL-1586) from all blood plasma

220 and mucosal swabs, and BAL samples. Briefly, increasing 10-fold dilutions of the samples were adsorbed to

221 Vero E6 cell monolayers in duplicate wells (200 µl). Cells were overlaid with EMEM agar medium plus 1.25%

222 Avicel, incubated for 2 days, and plaques were counted after staining with 1% crystal violet in formalin. The limit

223 of detection for this assay is 25 PFU/ml.

224

225 *Hematology and serum biochemistry*

226 Total white blood cell counts, white blood cell differentials, red blood cell counts, platelet counts, hematocrit

227 values, total hemoglobin concentrations, mean cell volumes, mean corpuscular volumes, and mean corpuscular

228 hemoglobin concentrations were analyzed from blood collected in tubes containing EDTA using a Vetscan HM5

229 hematologic analyzer (Abaxis). Serum samples were tested for concentrations of albumin, amylase, alanine

230 aminotransferase (ALT), aspartate aminotransferase (AST), alkaline phosphatase (ALP), blood urea nitrogen

231 (BUN), calcium, creatinine (CRE), C-reactive protein (CRP), gamma-glutamyltransferase (GGT), glucose, total

232 protein, and uric acid by using a Piccolo point-of-care analyzer and Biochemistry Panel Plus analyzer discs

233 (Abaxis). Partial pressures of CO_2 and O_2 were obtained using an iSTAT Alinity hematological analyzer (Abbott).

234

235 *ELISA*

236 Sera collected at the indicated time points were tested for SARS-CoV-2-specific immunoglobulin G (IgG)

237 antibodies by ELISA. MaxiSorp clear flat-bottom 96-well plates (44204 ThermoFisher, Rochester, NY) were

238 coated overnight with a 1:1000 dilution of irradiated SARS-CoV-2 infected or normal Vero E6 lysate in PBS, pH

239 7.4 kindly provided by Dr. Thomas W. Ksiazek (UTMB). Sera were initially diluted 1:100 and then four-fold

240 through 1:6400 in 3% BSA in 1✕ PBS. After a one-hour incubation, plates were washed six times with wash buffer

241 (1 x PBS with 0.2% Tween-20) and incubated for an hour with a 1:2500 dilution of horseradish peroxidase (HRP)-

242 conjugated anti-primate IgG antibody (Fitzgerald Industries International, Acton, MA). RT SigmaFast O-

243 phenylenediamine (OPD) substrate (P9187, Sigma, St. Louis, MO) was added to the wells after six additional

10

244 washes to develop the colorimetric reaction. The reaction was stopped with 3M sulfuric acid 5-10 minutes after

245 OPD addition and absorbance values were measured at a wavelength of 492nm on a spectrophotometer

246 (Molecular Devices Emax system, Sunnyvale, CA). Absorbance values were normalized by subtracting normal

247 wells from antigen-coated wells at the corresponding serum dilution. A sumOD value > 0.6 was required to

248 denote a positive sample. End-point titers were defined as the reciprocal of the last adjusted serum dilution with

249 a value ≥ 0.20.

250

251 *Serum neutralization assay*

252 Neutralization titers were calculated by determining the dilution of serum that reduced 50% of plaques ($PRNT_{50}$).

253 We incubated a standard 100 PFU amount of SARS-CoV-2 with two-fold serial dilutions of serum samples for

254 one hour. The virus-serum mixture was then used to inoculate Vero E6 cells for 60 minutes. Cells were overlaid

255 with EMEM agar medium plus 1.25% Avicel, incubated for 2 days, and plaques were counted after staining with

256 1% crystal violet in formalin.

257

258 *Bead-based cytokine and coagulation immunoassays*

259 Concentrations of immune mediators and fibrinogen were determined by flow cytometry using LegendPlex

260 multiplex technology (BioLegend). Serum levels of cytokines/chemokines and plasma levels of fibrinogen were

261 quantified using a Nonhuman Primate Inflammation 13-plex (1:4 dilution) or Human Fibrinolysis (1:10,000

262 dilution) panel, respectively. Samples were processed in duplicate following the kit instructions and

263 recommendations. Following bead staining and washing, 1500-4000 bead events were collected on a FACS

264 Canto II cytometer (BD Biosciences) using BD FACS Diva software. The raw .fcs files were analyzed with

265 BioLegend's cloud-based LEGENDplex™ Data Analysis Software.

266

267 *Histopathology and immunohistochemistry*

268 Necropsy was performed on all subjects euthanized at day 5. Tissue samples of all major organs were collected

269 for histopathologic and immunohistochemical (IHC) examination and were immersion-fixed in 10% neutral

270 buffered formalin. Specimens were processed and embedded in paraffin and sectioned at 5 μm thickness. For

271 IHC, specific anti-SARS immunoreactivity was detected using an anti-SARS nucleocapsid protein rabbit primary

11

272 antibody at a 1:800 dilution for 60 minutes (Novusbio NB100-56683). The tissue sections were processed for

273 IHC using the ThermoFisher Scientific Lab Vision Autostainer 360 (ThermoFisher Scientific). Secondary antibody

274 used was biotinylated goat anti-rabbit IgG (Vector Laboratories, Burlingame, CA) at 1:200 for 30 minutes

275 followed by Vector Streptavidin Alkaline Phosphatase at a dilution of 1:200 for 20 min (Vector Laboratories,

276 Burlingame, CA). Slides were developed with Bio-Red (Biopath) for 7 minutes and counterstained with

277 hematoxylin for one minute.

278 SARS-CoV-2 RNA *in situ* hybridization (ISH) in formalin-fixed paraffin embedded (FFPE) tissues was

279 performed using the RNAscope 2.5 high definition (HD) RED kit (Advanced Cell Diagnostics, Newark, CA)

280 according to the manufacturer's instructions. 20 ZZ probe pairs targeting the genomic SARS-CoV-2 spike protein

281 (S) gene were designed and synthesized by Advanced Cell Diagnostics (catalogue 848561). After sectioning,

282 deparaffinization with xylene and graded ethanol washes and peroxidase blocking, the sections were heated in

283 RNAscope target retrieval reagent buffer (Advanced Cell Diagnostics catalogue 322000) for 15 minutes and then

284 air-dried overnight. The sections were then digested with Protease III (catalogue 322340) at 40C in the HybEZ

285 oven (HybEZ, Advanced Cell Diagnostics catalogue 321711) for 15 minutes. Sections were exposed to ISH

286 target probe and incubated at 40C in the HybEZ oven for 2 hours. After rinsing, the signal was amplified using

287 the manufacturer provided pre-amplifier and amplifier conjugated to alkaline phosphatase and incubated with a

288 red substrate-chromogen solution for 10 minutes, counterstained with hematoxylin, air-dried, and cover slipped.

289

290 *Acknowledgments*

299

References

1. Organization, W.H. *Coronavirus disease (COVID-19) Situation Report – 117.* 2020 May 16, 2020]; Available from: https://www.who.int/docs/default-source/coronaviruse/situation-reports/20200516-covid-19-sitrep-117.pdf?sfvrsn=8f562cc_2.

2. Tseng, C.T., et al., *Immunization with SARS coronavirus vaccines leads to pulmonary immunopathology on challenge with the SARS virus.* PLoS One, 2012. **7**(4): p. e35421.

3. Bolles, M., et al., *A double-inactivated severe acute respiratory syndrome coronavirus vaccine provides incomplete protection in mice and induces increased eosinophilic proinflammatory pulmonary response upon challenge.* J Virol, 2011. **85**(23): p. 12201-15.

4. Weingartl, H., et al., *Immunization with modified vaccinia virus Ankara-based recombinant vaccine against severe acute respiratory syndrome is associated with enhanced hepatitis in ferrets.* J Virol, 2004. **78**(22): p. 12672-6.

5. Liu, L., et al., *Anti-spike IgG causes severe acute lung injury by skewing macrophage responses during acute SARS-CoV infection.* JCI Insight, 2019. **4**(4).

6. Gorbalenya, A.E., et al., *The species Severe acute respiratory syndrome-related coronavirus: classifying 2019-nCoV and naming it SARS-CoV-2.* Nature Microbiology, 2020. **5**(4): p. 536-544.

7. Bao, L., et al., *The pathogenicity of SARS-CoV-2 in hACE2 transgenic mice.* Nature, 2020.

8. Chan, J.F.-W., et al., *Simulation of the clinical and pathological manifestations of Coronavirus Disease 2019 (COVID-19) in golden Syrian hamster model: implications for disease pathogenesis and transmissibility.* Clinical Infectious Diseases, 2020.

9. Kim, Y.I., et al., *Infection and Rapid Transmission of SARS-CoV-2 in Ferrets.* Cell Host Microbe, 2020.

10. Rockx, B., et al., *Comparative pathogenesis of COVID-19, MERS, and SARS in a nonhuman primate model.* Science, 2020.

11. Munster, V.J., et al., *Respiratory disease and virus shedding in rhesus macaques inoculated with SARS-CoV-2.* bioRxiv, 2020: p. 2020.03.21.001628.

12. Shan, C., et al., *Infection with Novel Coronavirus (SARS-CoV-2) Causes Pneumonia in the Rhesus Macaques.* 2020, Research Square.

13. Yu, P., et al., *Age-related rhesus macaque models of COVID-19.* Animal Models and Experimental Medicine, 2020. **3**(1): p. 93-97.

14. McAuliffe, J., et al., *Replication of SARS coronavirus administered into the respiratory tract of African Green, rhesus and cynomolgus monkeys.* Virology, 2004. **330**(1): p. 8-15.

15. Letko, M., A. Marzi, and V. Munster, *Functional assessment of cell entry and receptor usage for SARS-CoV-2 and other lineage B betacoronaviruses.* Nat Microbiol, 2020. **5**(4): p. 562-569.

16. Shang, J., et al., *Cell entry mechanisms of SARS-CoV-2.* Proc Natl Acad Sci U S A, 2020.

17. Capobianchi, M.R., et al., *Molecular characterization of SARS-CoV-2 from the first case of COVID-19 in Italy.* Clin Microbiol Infect, 2020.

18. Herold, T., et al., *Level of IL-6 predicts respiratory failure in hospitalized symptomatic COVID-19 patients.* medRxiv, 2020: p. 2020.04.01.20047381.

19. Connors, J.M. and J.H. Levy, *COVID-19 and its implications for thrombosis and anticoagulation.* Blood, 2020.

20. Ranucci, M., et al., *The procoagulant pattern of patients with COVID-19 acute respiratory distress syndrome.* J Thromb Haemost, 2020.

21. Williamson, B.N., et al., *Clinical benefit of remdesivir in rhesus macaques infected with SARS-CoV-2.* bioRxiv, 2020: p. 2020.04.15.043166.

22. Geisbert, T.W., et al., *Development of an Acute and Highly Pathogenic Nonhuman Primate Model of Nipah Virus Infection.* PLOS ONE, 2010. **5**(5): p. e10690.

23. Callow, K.A., et al., *The time course of the immune response to experimental coronavirus infection of man.* Epidemiol Infect, 1990. **105**(2): p. 435-46.

24. Galanti, M. and J. Shaman, *Direct observation of repeated infections with endemic coronaviruses.* medRxiv, 2020: p. 2020.04.27.20082032.

25. Weinstock, M.E., Ana; Russell, Joshua W.; Leib,Ari; Miller, Jordan A.; Cohen, David J.; Waite, Stephen; Frye, Allen; Illuzzi;Frank A., *Chest X-Ray Findings in 636 Ambulatory Patients with COVID-19 Presenting to an Urgent Care Center: A Normal Chest X-Ray Is no Guarantee.* J Urgent Care Med., 2020. **14**(7): p. 13-18.

26. Qi, F., et al., *Single cell RNA sequencing of 13 human tissues identify cell types and receptors of human coronaviruses.* Biochemical and Biophysical Research Communications, 2020. **526**(1): p. 135-140.
27. Diao, B., et al., *Human Kidney is a Target for Novel Severe Acute Respiratory Syndrome Coronavirus 2 (SARS-CoV-2) Infection.* medRxiv, 2020: p. 2020.03.04.20031120.
28. Chen, X., et al., *Detectable serum SARS-CoV-2 viral load (RNAaemia) is closely correlated with drastically elevated interleukin 6 (IL-6) level in critically ill COVID-19 patients.* Clin Infect Dis, 2020.
29. CDC. *Coronavirus Disease 19 (COVID-19).* 2020 [cited 2020 16 May]; Available from: https://www.cdc.gov/coronavirus/2019-ncov/lab/rt-pcr-panel-primer-probes.html.

387 **Figure 1: Hematological features of AGMs infected with SARS-CoV-2.** Blood was collected from AGMs on
388 procedure days (0, 2, 3, 4, 5, 7, 9, 12, 15, 21). Partial pressures of CO_2 and O_2 were obtained using an iSTAT
389 Alinity hematological analyzer (Abbott). Leukocyte subpopulations and thrombocytes were differentiated and
390 quantified using a Vetscan HM5 hematological analyzer (Abaxis). Serum analytes (ALT, AST, ALP, CRP) were
391 quantified using a Piccolo serum biochemistry analyzer (Abaxis). For all graphs, dashed lines and open
392 symbols (AGM-1, AGM-2, AGM-3) indicate AGMs sacrificed 5 dpi; solid lines (AGM-4, AGM-5, AGM-6)
393 indicate AGMs held to 21 dpi.
394

395

15
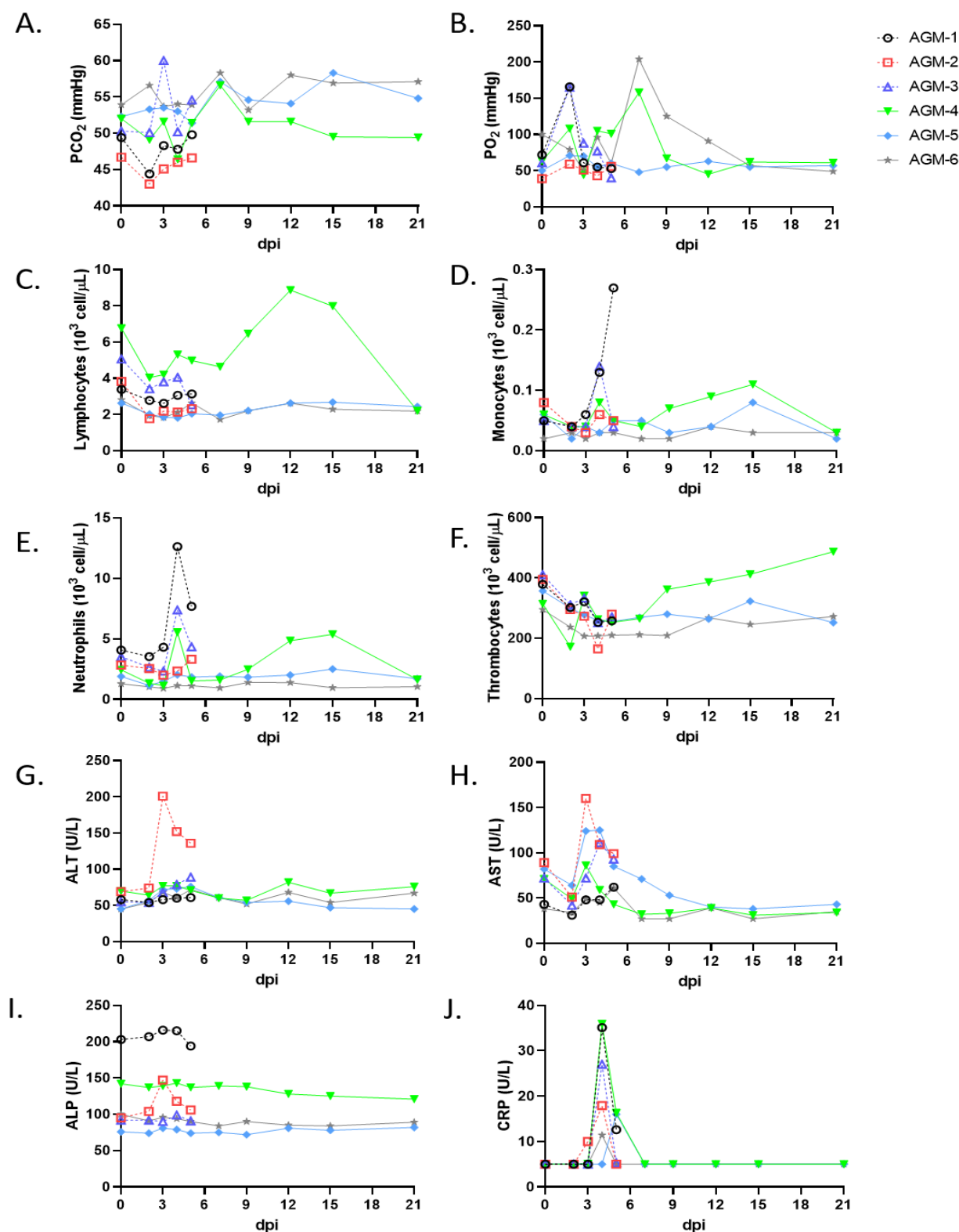
Figure 2: Lung gross pathology in SARS-CoV-2-infected AGMs. Side and dorsal views of lungs from AGMs sacrificed 5 dpi after infection with SARS-CoV-2 exhibiting marked pulmonary consolidation with hemorrhage, ranging from multifocal to locally extensive in severity. **(A)** and **(B)** are dorsal and side views of the lungs from AGM-1. **(C)** and **(D)** are dorsal and side views of the lungs from AGM-2. **(E)** and **(F)** are dorsal and side views of the lungs from AGM-3.
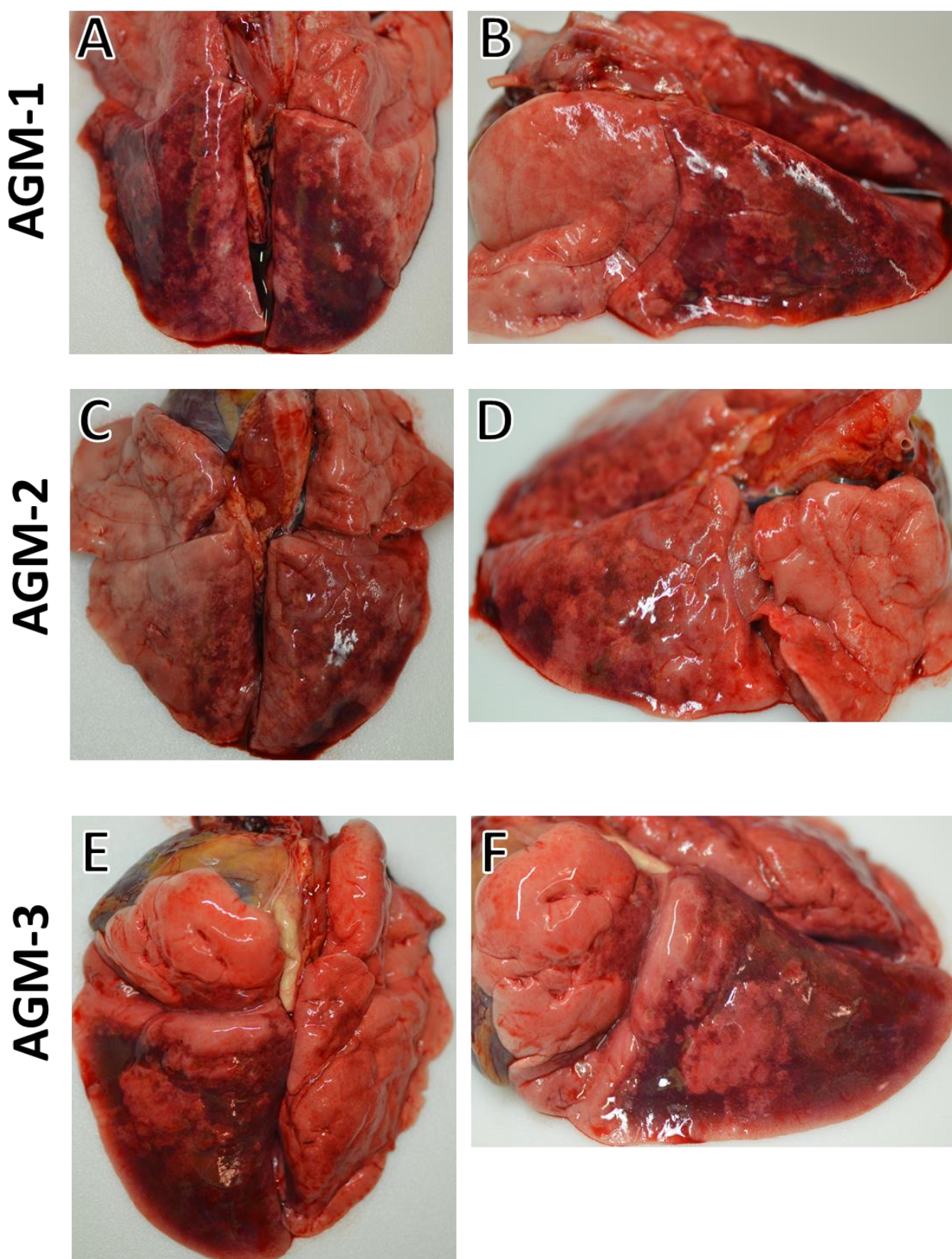
Figure 3: Pulmonary histologic changes in AGMs infected with SARS-CoV2 (A) Low magnification image displaying the marked acute bronchiolitis and interstitial pneumonia (4x) (B) Higher magnification image displaying multiple multinucleated giant cells (>) and acute bronchiolitis with edema and hemorrhage (40x) (C) Terminal bronchioles with multiple fibrous tissue proliferations reminiscent of bronchiolitis obliterans organizing pneumonia (BOOP)-like lesions (*) (20x) (D) Multiple multinucleated giants cells (>) within terminal bronchioles of lesser affected monkey (40x) (E) SARS-CoV 2 positive immunohistochemical (IHC) labeling (red) of alveolar macrophages and pneumoncytes within acute bronchiolar inflammation (20x) (F) SARS-CoV 2 positive IHC labeling (red) of type I (>) and type II (=>) pneumocytes (40x) (G) SARS-CoV 2 positive IHC labeling (red) of respiratory epithelium (40x), (H) Genomic SARS-CoV2 RNA (red) detected by *in situ* hybridization in a cluster of cells associated with acute bronchiolitis (60x).

17
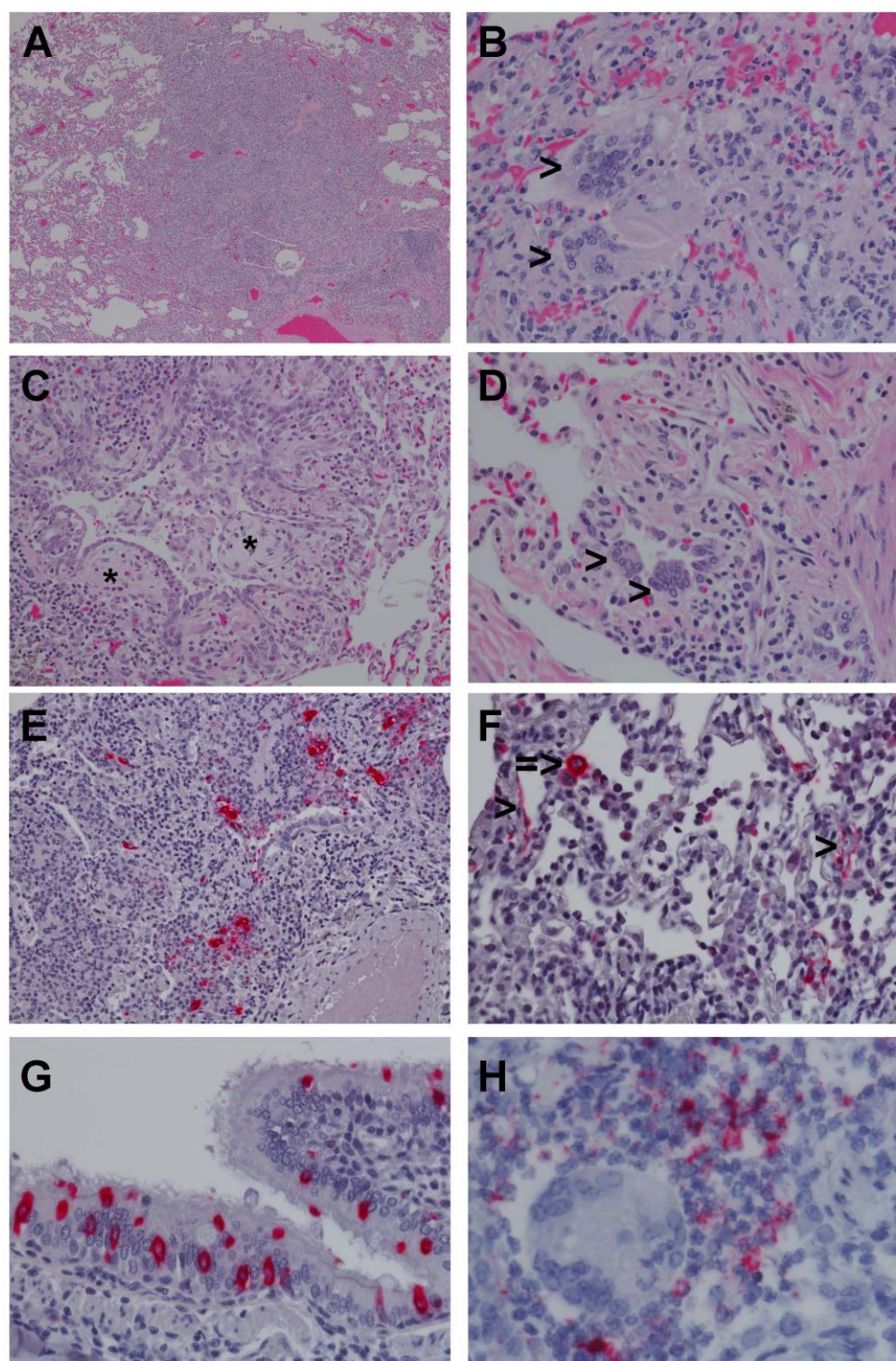
Figure 4: Detection of SARS-CoV-2 vRNA and infectious virus in muscosal swabs and BAL fluid. RNA extracted from swabs of mucosa and BAL fluid from AGMs infected with SARS-CoV-2 was subjected to RT-qPCR analysis or viral titration. **(A,B)** nasal swabs, **(C,D)** oral swabs, **(E,F)** rectal swabs, **(G,H)** BAL fluid. For all graphs, dashed lines and open symbols (AGM-1, AGM-2, AGM-3) indicate AGMs sacrificed 5 dpi; solid lines (AGM-4, AGM-5, AGM-6) indicate AGMs held to 21 dpi. Data plotted is the mean of duplicate RT-qPCR reactions or duplicate wells.

18
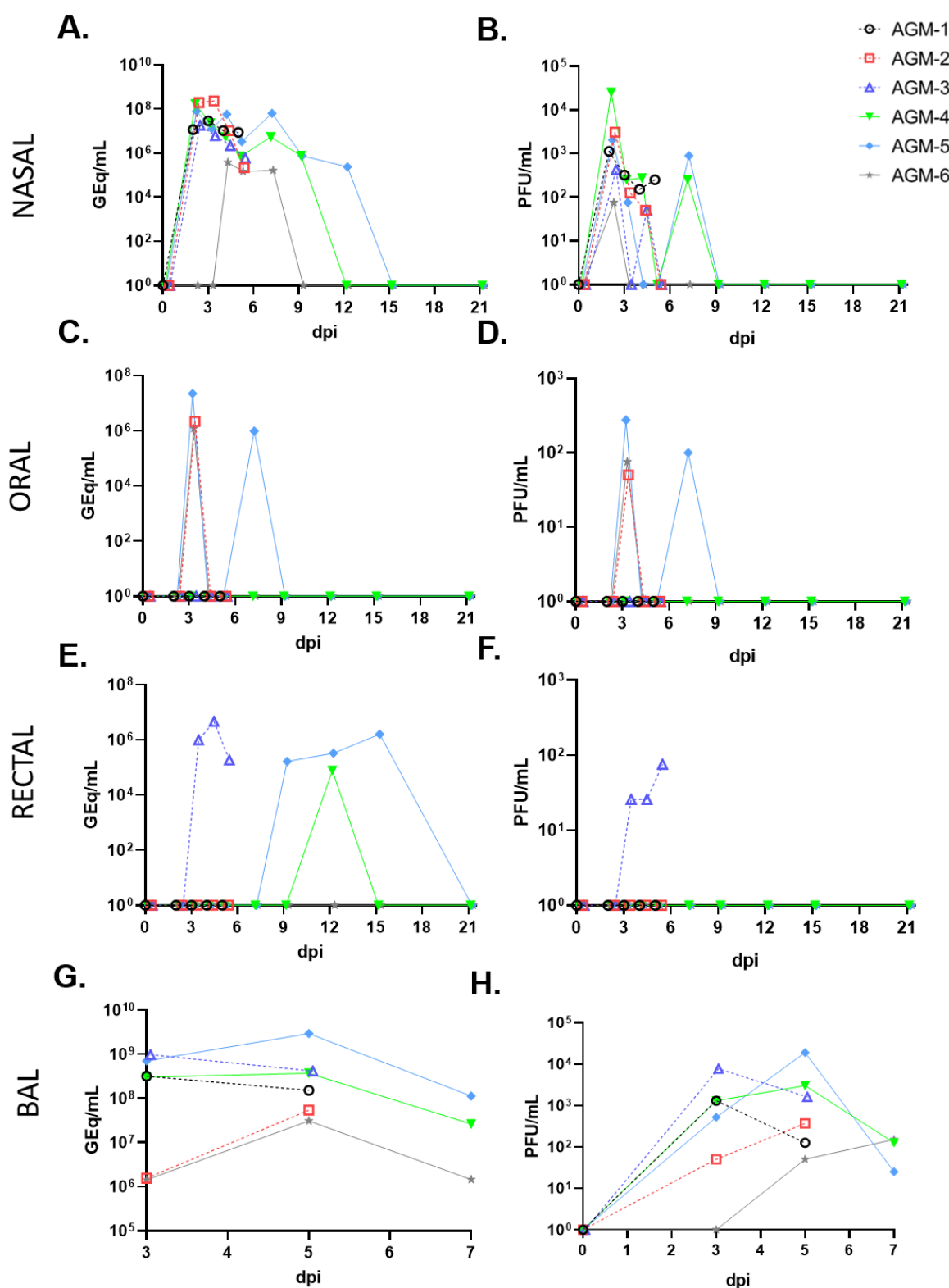
420 **Figure 5: Soluble markers of inflammation detected in SARS-CoV-2 infected AGM sera over the course**
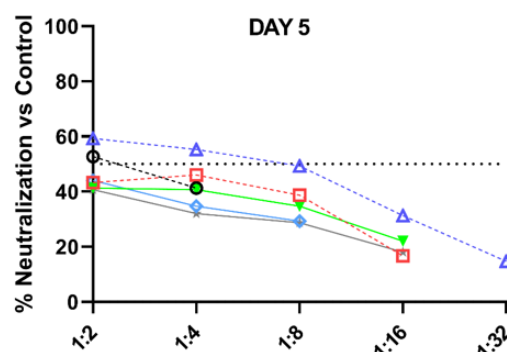
421 **of the study**

422
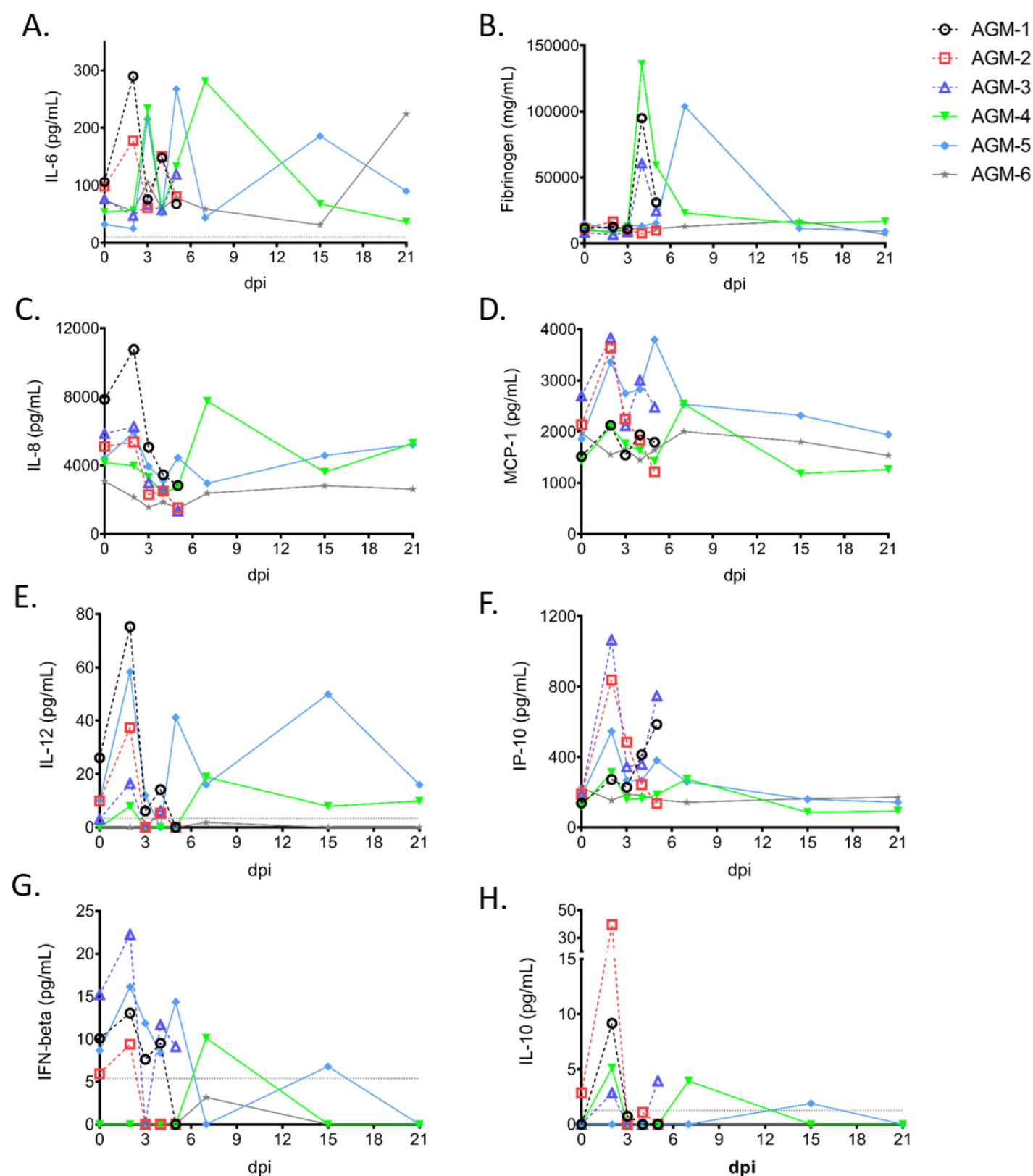
Figure 6: Serum anti-SARS-CoV-2 antibody titers and virus neutralization in AGMs. Anti-SARS-CoV-2 IgG binding titers were determined using traditional ELISA methodology where the antigen was whole infected cell lysate (background subtraction was performed using virus negative cell lysate) and titers are represented as reciprocal dilutions (**A**.). Antibody neutralization titers were also determined for sera collected 5 dpi (**B**), 7 dpi (**C**), 15 dpi (**D**), and 21 dpi (**E**). Data plotted represents the percent reduction in plaque counts (average of duplicate wells) compared to the average of three independent virus control plates (average plaque count across all three plates = 75). Dashed lines on each graph indicate 50% neutralization compared to the virus control plates. All plaque counts were calculated from duplicate wells at each dilution.
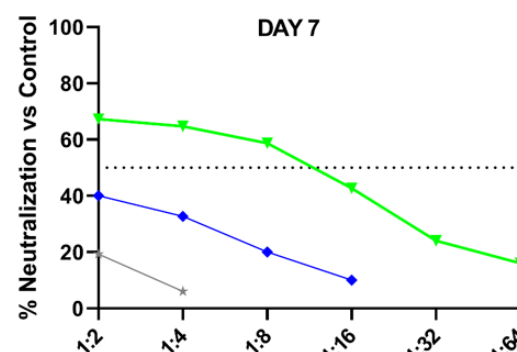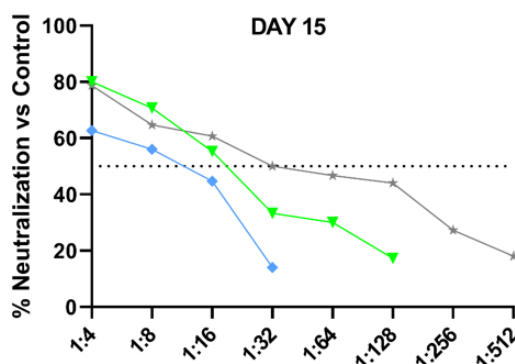

20